Publication title	Design guidelines for laser powder bed fusion in Inconel 718
Authors	Herzog, Dirk; Asami, Mohammad Karim; Scholl, Christoph; Ohle, Christoph; Emmelmann, Claus; Sharma, Ashish N.; Markovic, Nick; Harris, Andy
Issue Date	December 28, 2021
Publisher	Laser Inst. of America
Type of publication	Journal Article
Acknowledgement	This project has received funding from the Clean Sky 2 Joint Undertaking (JU) under grant agreement No 831872. The JU receives support from the European Union's Horizon 2020 research and innovation programme and the Clean Sky 2 JU members other than the Union
Disclaimer	

Design guidelines for laser powder bed fusion in Inconel 718

Cite as: J. Laser Appl. **34**, 012015 (2022); https://doi.org/10.2351/7.0000508
Submitted: 02 July 2021 • Accepted: 29 November 2021 • Published Online: 28 December 2021

Dirk Herzog, Karim Asami, Christoph Scholl, et al.

Journal of Laser Applications ARTICLE scitation.org/journal/jla

Design guidelines for laser powder bed fusion in Inconel 718

Cite as: J. Laser Appl. **34**, 012015 (2022); doi: 10.2351/7.0000508
Submitted: 2 July 2021 · Accepted: 29 November 2021 ·
Published Online: 28 December 2021

Dirk Herzog,[1] Karim Asami,[1] Christoph Scholl,[1] Christoph Ohle,[1] Claus Emmelmann,[1] Ashish Sharma,[2] Nick Markovic,[3] and Andy Harris[3]

AFFILIATIONS

[1]Institute of Laser and Systems Technology, Hamburg University of Technology, Denickestr. 17, 21073 Hamburg, Germany
[2]GE Aviation, Advanced Aviation Technology, Freisinger Landstrasse 50, 85748 Garching bei München, Germany
[3]Autodesk Research, Autodesk Ltd., 6 Agar Street, London WC2N 4HN, United Kingdom

Note: Paper published as part of the special topic on Proceedings of the International Congress of Applications of Lasers & Electro-Optics 2021.

ABSTRACT

Additive manufacturing (AM) has been leveraged across various industries to potentially open design spaces allowing the design of parts to reduce the weight, cost, and integrated design. Over the past decade, AM has sped up fast enough to penetrate various industry offering potential solutions for multiple materials, such as metals, alloys, plastics, polymers, etc. However, challenges lie to best utilize the opened design spaces as current generation engineers are trained to design parts for the conventional manufacturing process. With this lack of design guidelines for the AM process, users are limiting themselves to best utilize the offering made by advanced manufacturing. For aerospace parts, the design freedom of additive manufacturing is attractive mainly for two purposes: for weight reduction through lighter, integrated design concepts as well as for functional optimization of parts aiming at an increase of performance, e.g., by optimizing flow paths. For both purposes, it is vital to understand the material-specific and manufacturing process design limits. In AM, combination of each material and manufacturing process defines the design space by influencing minimum thickness, angle, roughness, etc. This paper outlines a design guideline for the laser powder bed fusion (also DMLM, direct metal laser melting) AM process with Inconel 718 material. Inconel 718 is a superalloy with superior mechanical properties and corrosion resistance at elevated temperatures up to 700 °C and is, therefore, used in several applications including aerospace engine parts. Due to its weldability, the alloy has also been extensively investigated in laser powder bed fusion and other additive manufacturing processes. A comprehensive study is provided both analytically and experimentally suggesting how parts can be designed having critical design features, manufacturing direction/orientation to meet design requirements, design accuracy, and quality. Design features presented include walls, overhangs, bore holes, and teardrop shapes, with their minimal feature sizes and effects on accuracy and roughness of the build parts. For the light-weight design of parts, different concepts such as lattices and stiffener structures are discussed. For gas or liquid carrying flow channels, the geometrical form and size are highlighted. Based on an approach by Kranz *et al.*, design guidelines for Inconel 718 are derived from the experiments and provided in the form of a catalog for easy application.

Key words: Design for additive manufacturing, IN718, laser powder bed fusion, Aerospace applications

I. INTRODUCTION

Nickel-based superalloys are used today in a broad range of industrial and, especially, aerospace applications due to their high strength and corrosion resistance at higher temperatures. A variety of alloys exists, some of which are specifically designed for use in cast, wrought, and powder metallurgical production routes.[1]

One of these alloys is Inconel 718 (IN718), which is typically wrought or processed in powder bed fusion due to its weldability,

TABLE I. Selected design features.

Unsupported small walls

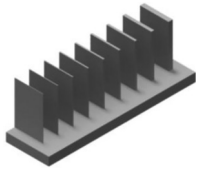

Width (mm)	10
Height (mm)	15
Thickness (mm)	0.1, 0.2, … , 0.7/1.0/1.5

Unsupported large walls

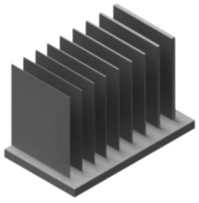

Width (mm)	25
Height (mm)	30
Thickness (mm)	0.1, 0.2, … , 0.7/1.0/1.5

Supported walls

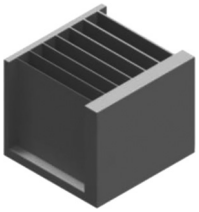

Width (mm)	30
Height (mm)	30
Thickness (mm)	0.1, 0.2, … , 0.7

Inclined walls

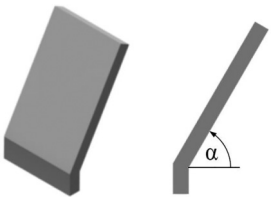

Width (mm)	20
Height (mm)	30
Thickness (mm)	3
Overhang angle α (°)	25, 30, … , 70/80

TABLE I. (*Continued.*)

Horizontal overhangs

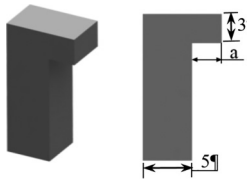

Width (mm)	5
Height (mm)	14
Total length (mm)	5 + a
Overhang length a (mm)	0.5, 1.0, … , 3.0

Horizontal bridges

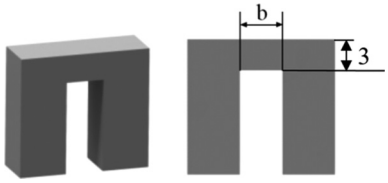

Width (mm)	5
Height (mm)	11/14/17
Total length (mm)	10 + b
Bridge span b (mm)	1, 2, … , 5

Unsupported bars

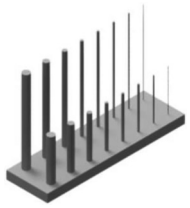

Height (mm)	15, 30
Diameter D (mm)	0.2, 0.4, … , 1.0/1.5/2.0/2.5

Horizontal bore holes

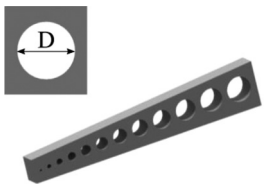

Width (mm)	10
Diameter D (mm)	1.0, 2.0, … , 12.0
Horizontal tear drop features	

TABLE I. (*Continued.*)

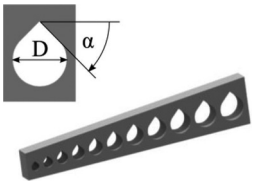

Width (mm)	10
Angle α (°)	30, 45
Diameter D (mm)	5, 6, … , 15

and it is particularly used in gas turbine blades,[2] combustors, and turbocharger rotors,[1] just to name a few applications.

Additive manufacturing is used in the aerospace industry typically to optimize parts regarding weight and functionality,[3,4] using its high degree of design freedom.[5] Still, each AM process features its remaining design restrictions.[6] To exploit the full potential and avoid production waste and costs, the designer needs to know the exact design limits of the technology for a given material as part of a holistic design for additive manufacturing (DfAM) approach.

Therefore, several research groups have been working on establishing design guidelines for AM processes and specific materials such as the commonly used titanium alloy Ti-6Al-4V.[7,8]

The work presented by Kranz *et al.*[7] provides specific design limits for typical part features, such as walls, bar structures, bore holes, and the like, specifically for laser powder bed fusion (L-PBF) of Ti-6Al-4V, and also provides some more general recommendations, such as the orientation of parts toward the recoater angle.

Therefore, this article builds on the mentioned design guidelines and identifies the corresponding design limits for design features build-out of IN718 and discusses its application to the DfAM of an aerospace engine frame.

II. MATERIALS AND METHODS

In the following, the selected design features are presented. As the design limits discussed in this paper will be valid for a specific machine, material, and process parameter combination, the material and process conditions are described as well.

TABLE II. Elemental composition of the received IN718 powder.

Element	C	S	Cr	Ni	Mn
wt. %	0.02	0.001	18.2	53.9	0.04
Element		Si	Mo	Ti	Nb
wt. %		0.08	3.0	0.98	5.27
Element		Cu	Fe	P	Al
wt. %		0.03	Bal.	0.009	0.5
Element		Pb	Co	B	Ta
wt. %		0.0002	0.2	0.004	0.01

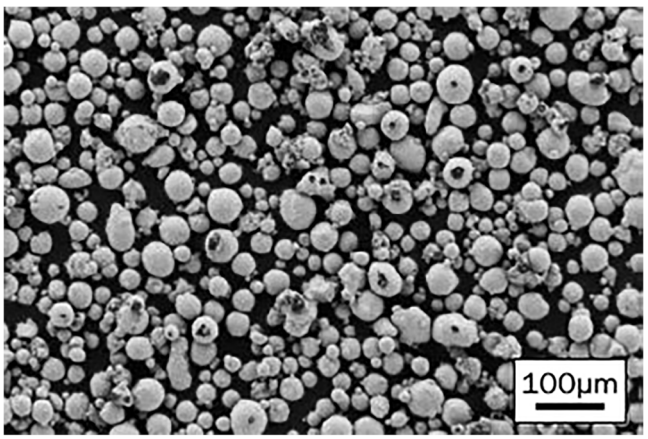

FIG. 1. Particle visualization of the IN718 powder.

A. Design features and reference geometries

Based on the literature,[7,9] nine different features have been identified that represent basic, typical design elements used in the manufacturing of parts. Each feature can be varied with one or two geometrical parameters to identify the design limits, e.g., for wall thicknesses, overhang angles, etc. Table I shows the selected design elements and sizes, including the range for the geometrical parameter variation per element.

B. Materials

For the fabrication of the specimens, IN718 powder (VDM Metals International GmbH, Unna, Germany) with the composition specified by the manufacturer provided in Table II has been used. The particle size distribution was monomodal with D10 = 24.2 μm, D50 of 39.2 μm, and D90 of 57.8 μm. The particle shape was investigated using SEM and was found to be mostly spherical with a few satellite particles present (see Fig. 1).

C. L-PBF process

All specimens have been manufactured with L-PBF on a GE Additive M2 system (GE Additive, Lichtenfels, Germany). For productivity reasons, the layer thickness was set to l = 60 μm, while laser power P_L, scan speed v, and hatch distance h have been optimized for bulk density and roughness. The resulting parameter set is given in Table III.

TABLE III. Process parameters used for the specimen fabrication.

L-PBF system			
Parameter		Unit	GE additive M2
Laser power	P_L	W	280
Scan speed	V	m/s	1
Hatch	H	μm	95
Powder bed temp.	T_0	K	293.15
Layer thickness	L	μm	60

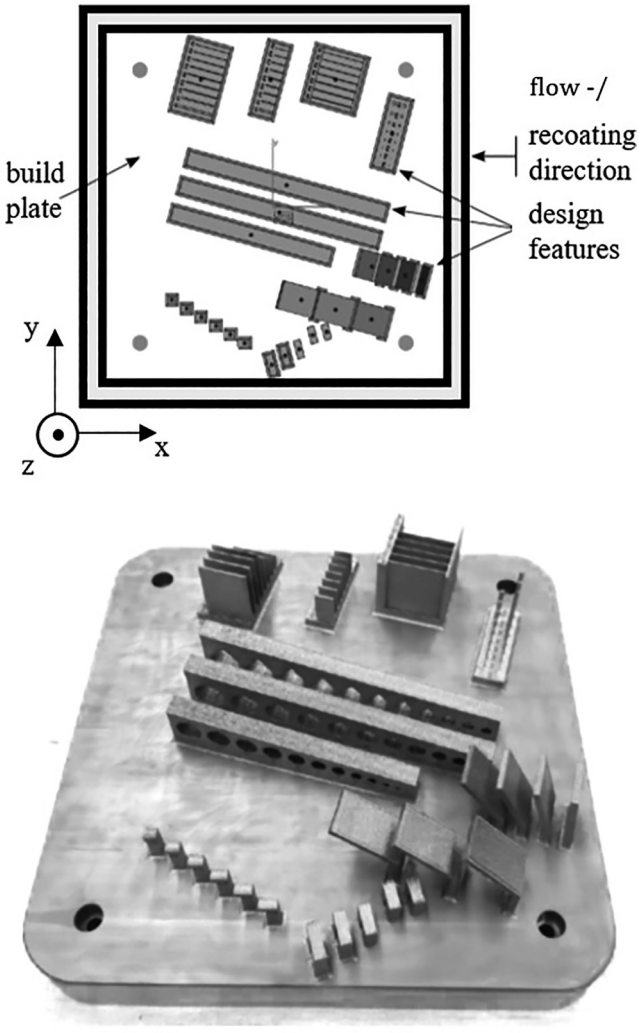

FIG. 2. Prepared build job (top) and as-printed (bottom).

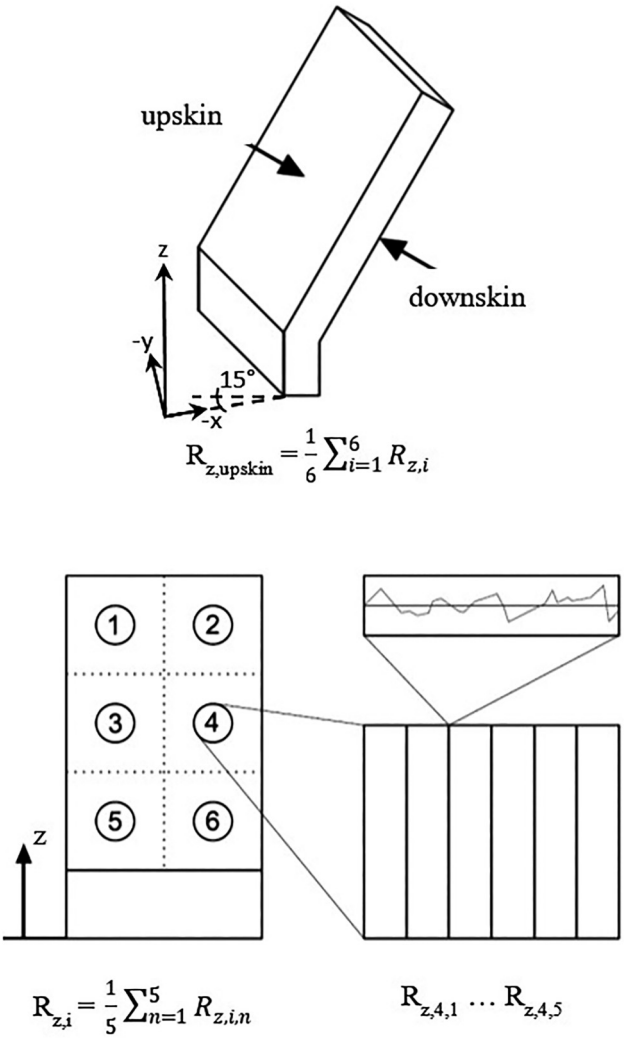

FIG. 3. Roughness evaluation on upskin and downskin areas, deriving mean R_z values.

To validate the parameters, tensile tests according to DIN EN ISO 6892-1 have been performed on a total of ten specimens manufactured from the same powder and parameters and machined to final geometry after L-PBF. Half of the specimens were tested in a build condition, resulting in an ultimate tensile strength of UTS = 1159 ± 52 MPa and an elongation at break of A = 37 ± 2%. This is in good agreement with the literature.[10] The other half of the specimens were subjected to a hot isostatic pressing (HIP, performed at Quintus Technologies Application Centre, Västerås, Sweden) according to ASTM F3055-14a (1120 °C/150 MPa/4 h) followed by quenching and a precipitation hardening (725 °C/150 MPa/8 h + 630 °C/10 h). After heat treatment, the UTS increased to UTS = 1504 ± 48 MPa with a reduced elongation at a break of A = 23 ± 2%. These values are also in good agreement with the literature, while the UTS is slightly superior to the values provided in the review of Hosseini and Popovich.[10]

For fabrication, the design features have been oriented on the build plate following the general guidelines by Kranz *et al.*[7] to avoid positioning filigree structures parallel to the recoater. Figure 2 shows an exemplary build job and the position of the specimens.

D. Roughness measurement

To evaluate the surface roughness of the design features, a 3D laser scanning microscope (VK-X100, Keyence, Osaka, Japan) is used. Measurements are performed on each relevant surface, evaluating the mean roughness R_z as a mean of individual R_z of

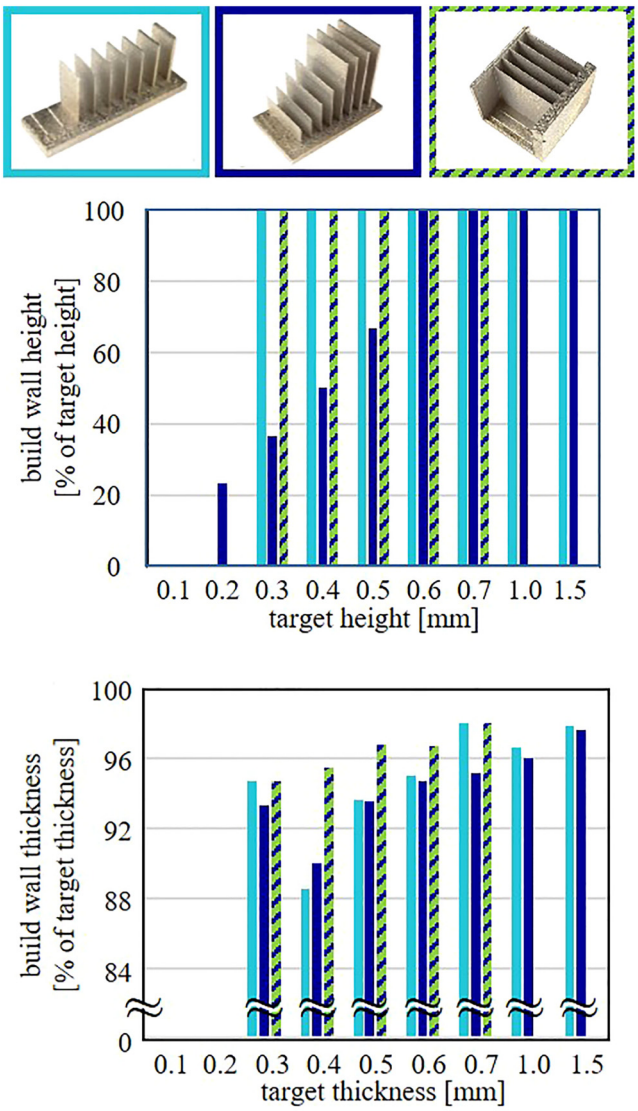

FIG. 4. Height (top) and thickness (bottom) measurements of the unsupported and supported walls.

five separate lines at six different measurement locations (cf. Fig. 3).

III. RESULTS AND DISCUSSION

The experimental measurements for the observed features are displayed in Figs. 4–8. In each diagram, the percentage target values have been plotted over the absolute target values except in the case of inclined walls. Here, the mean roughness is plotted over the inclination angle and will be described in the following.

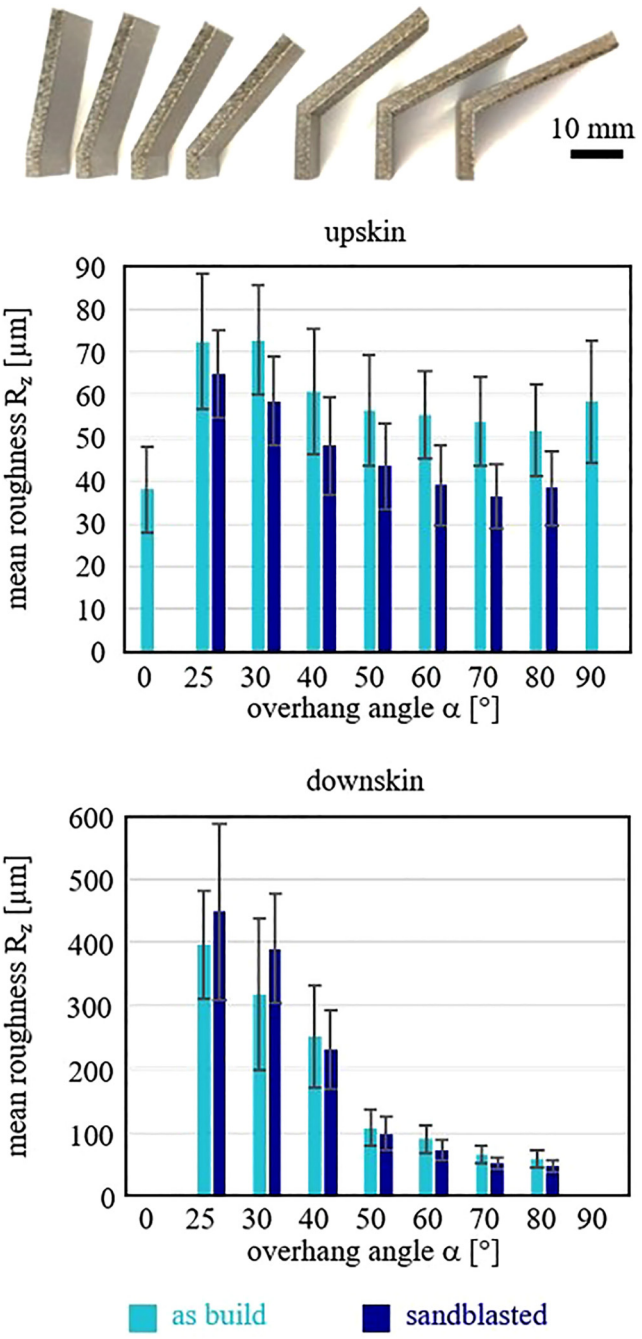

FIG. 5. Mean roughness of upskin (top) and downskin (bottom) surfaces in dependence of an overhang angle.

A. Supported and unsupported walls

Figure 4 shows the relative wall height and thickness over the target height and thickness for all as-built wall specimens as

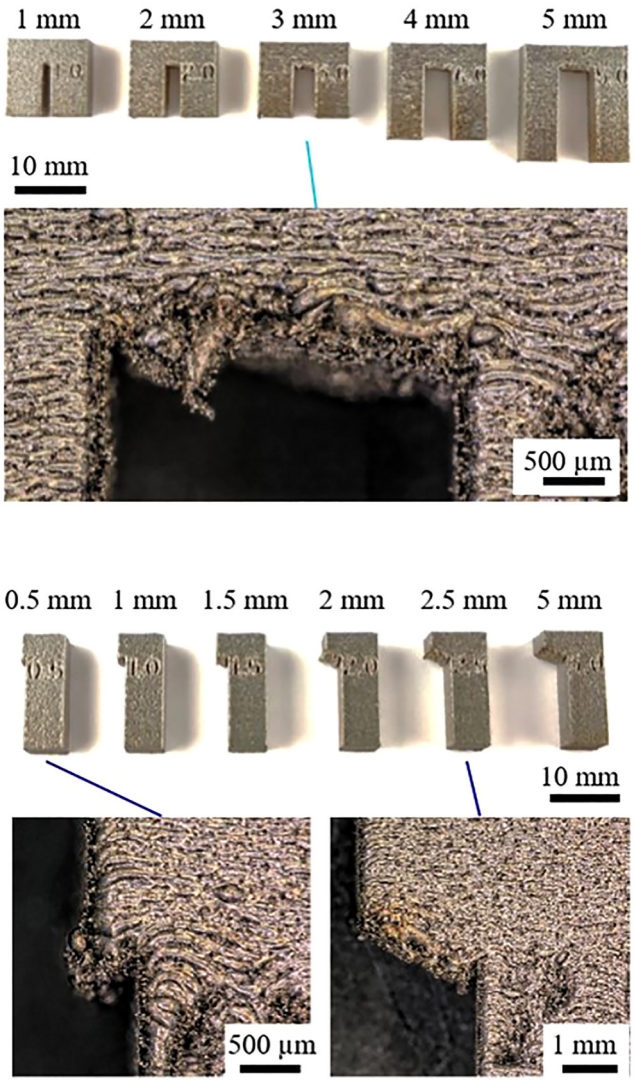

FIG. 6. Exemplary geometric deviations on bridge specimens (top) and overhang specimens (bottom).

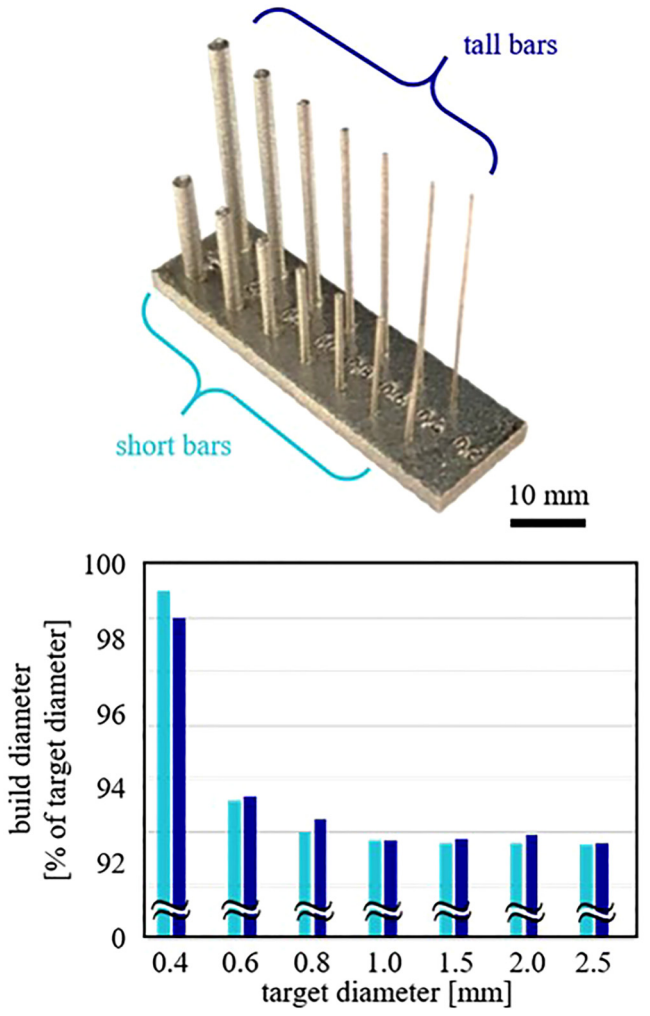

FIG. 7. Build diameter of the short (15 mm, light blue) and tall (30 mm, dark blue) bars.

described in Sec. II. Supported and unsupported walls with a target thickness of less than 0.3 mm and unsupported large walls with less than 0.6 mm were not built to full height.

All walls showed a lower wall thickness than the target value; however, walls with a thickness ≥0.6 mm consistently reached ≥95% of the target.

B. Inclined walls

All inclined wall specimens down to a 25° overhang angle were fully built, showing that the material and machine set-up combination produced very robust results (cf. Fig. 5). The mean roughness on the horizontal upskin surface was $R_z = 37.9\,\mu m$. Measurement of 0° and 90° overhang angles has been performed on the top and side of the bridge specimens. When inclined, the mean roughness increased to $R_z = 51.8–72.9\,\mu m$, with scattering higher than the influence of the angle itself. However, the roughness on the downskin surface was considerably higher reaching $R_z > 100\,\mu m$ for overhang angles $\alpha > 50°$.

C. Overhang and bridge features

All bridges could be built up (cf. Fig. 6); however, starting from a bridge span of $b \geq 3$ mm, considerable material fall-in on the downskin surface of the span is observed.

The overhang features could be realized up to $a = 1$ mm. Larger overhangs show a material fall-in, similar to the literature on Ti-6Al-4V.[7]

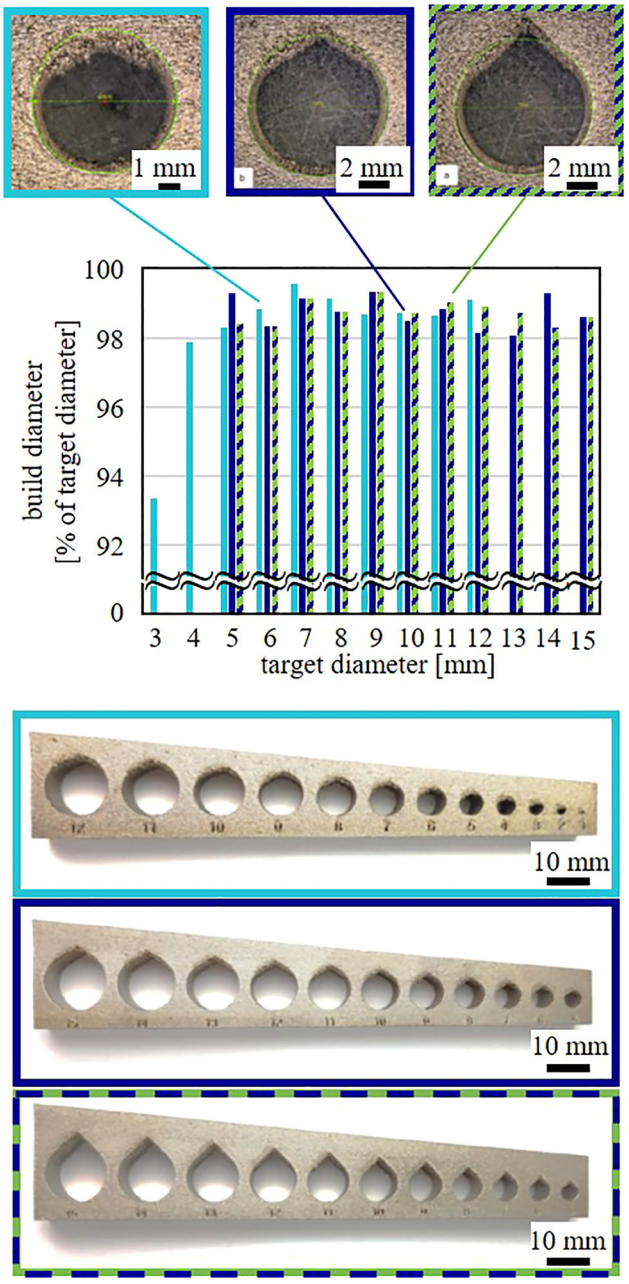

FIG. 8. Build diameter of circular bore holes (light blue) and tear drop-shaped holes with inclination angles of 30° (dark blue) and 45° (green).

D. Unsupported bars

The unsupported bar features (cf. Fig. 7) could be built for $d \geq 0.4$ mm. It was observed that bars with $d < 0.8$ mm are rather unstable and tend to bend during manufacture. All bars are built smaller than the target diameter. Both observations are invariant from the bar height and lead to the conclusion that for small structures, the focus diameter of the laser beam, the material parameter, and the scan strategy have to be modified to ensure a geometrical precise buildup.

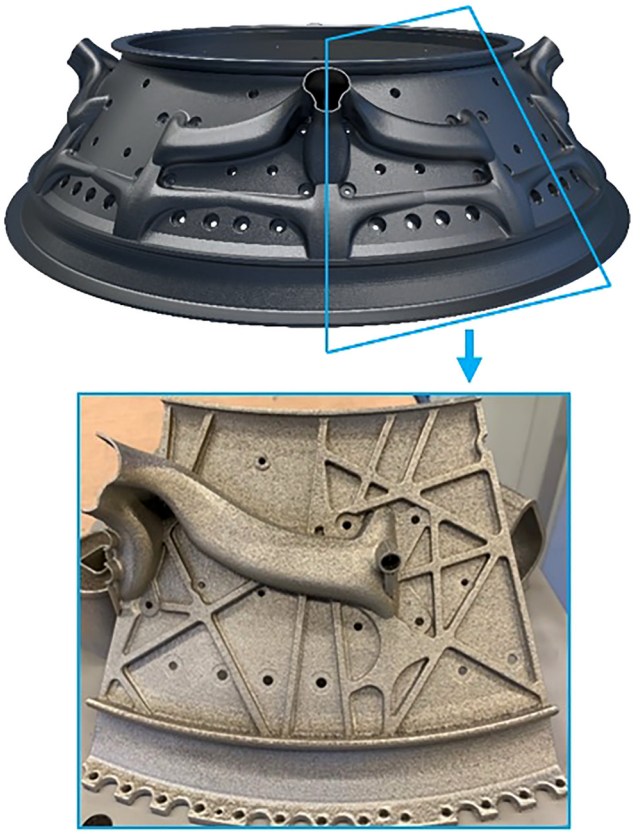

FIG. 9. Simplified model of a 360° large-scale engine frame (top) and a printed 1/8 segment (bottom).

E. Horizontal bore holes

Bore holes with circular and tear drop shapes are shown in Fig. 8. All holes can be manufactured, independent of the shape, but circular holes show higher material fall-in at the top. Therefore, support structures are recommended for circular holes. Holes with $d < 4$ mm also show high deviation in diameter. Tear drop shapes with $\alpha = 30°$ show a similar material fall-in for $d \geq 10$ mm. The tear drop shapes with $\alpha = 45°$, in contrast, show no significant material fall-in.

F. Application to light-weight design

The limits of the design features shown in this work can be transferred to the design of light-weight parts and concepts. For lattice structures, for example, a strut diameter of at least 0.4–0.6 mm should be chosen, and it should be noted that the actual build diameter is ~8% lower than the target value for $d \geq 0.6$ mm

for the combination of material parameter and machine setup used in these experiments, and an overhang angle of >25° must be avoided.

Stiffener structures may be designed within the limits of the wall thickness presented in Fig. 4. Gas or liquid carrying flow channels should be designed in a tear drop shape with an overhang angle of ≥30° on the top when possible to avoid internal supports.

Advancements in software optimization tools have allowed many of the design for additive manufacturing processes to be considered during the optimization process. Specific considerations can be given to a build angle to minimize support structure volume. The geometry can also be restricted to maintain access to surfaces that require machining and assembly, such as holes for fasteners. The optimization tools can then use this information alongside structural and thermal/fluid considerations to then create a geometry that meets manufacturing and also structural/fluid/thermal requirements.

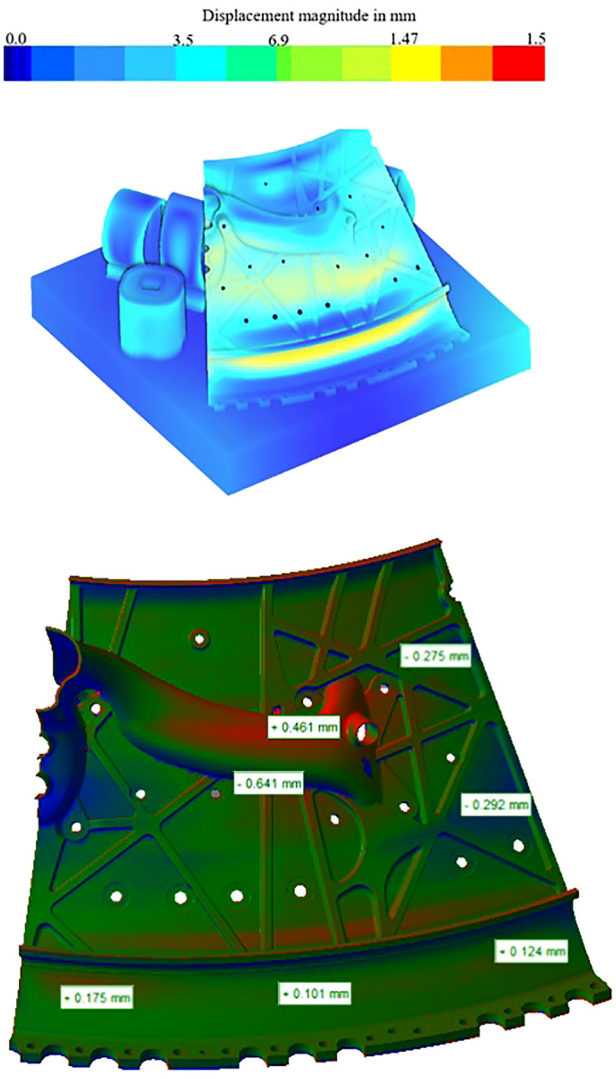

FIG. 10. Predicted build simulation displacements (top) and the displacement deviations between real and predicted results where red shows the maximum deviation (bottom).

Lattice structures are also an important consideration in design for additive manufacturing as they can offer further benefits to structural/fluid/thermal and manufacturing performance. The lattice structure can increase the stiffness of a design by increasing the second moment of area and reducing mass. Additive manufacturing of these structures also reduces distortion from thermal energy buildup and subsequent cooling.

With the knowledge of the design limits, a large-scale engine frame was selected as the demonstrator part. In a design for additive manufacturing (DfAM) approach, the main structure was optimized using generative design to minimize mass while maximizing the stiffness and meeting the strength requirements, while respecting manufacturing constraints. The manifold was optimized to minimize the system pressure loss within the allowed design space. A conformal lattice was applied inside the structure cavity to increase the stiffness to weight ratio while adhering to the aerothermal strength and fatigue requirements. Furthermore, consolidation of the hardware assembly from 150 parts to one monolithic structure was done. The lattice design has reduced the heat loss from the casing by separating the inner and outer walls of the casing. The wall thicknesses, bore holes, and the shape of the manifold section were kept within the limits of process capabilities applying the results from Sec. III A-E. Figure 9 shows the component as well as a printed 1/8 segment.

The optimized design reduced mass by 34%, and the pressure loss through the manifold system was calculated to have reduced by 91%. The manifold was fully attached to the casing to reduce the parasitic weight and increase the contribution of the structure to the case stiffness.

Simulation of the additive manufacturing process is also an important step as it can reduce the risk of failure during the build process from issues, such as recoater blade interference, support failure, and distortion. These can help inform the manufacturing process and also the design.

To prepare for manufacturing, a build preparation and build simulation were undertaken to understand the structural behavior and to find a support strategy for the build job. The process parameters and the type of support structures from a previous build job were used for the current design because the actual behavior versus the simulated behavior was well understood. The thermomechanical results predicted the deforming shape after build completion and predicted other failure modes. After the manufacturing was complete, the real deformation was measured using structure light scanning using an ATOS ScanBox, and this overlaid with the predicted deformation, shown in Fig. 10.

To conclude, the build simulation results did not predict any additive manufacturing issues. The re-coater interface was predicted to be at low risk. This assumption was validated because no visible re-coater marks were detected in Fig. 8. The difference between the real and predicted displacements was sufficiently small (461 μm) that there is high confidence in the simulation model prediction.

TABLE IV. Design guidelines and recommendations for L-PBF of IN718.

Geometry feature		Recommendation	
Name	Illustration	Value	Comment
Unsupported small walls	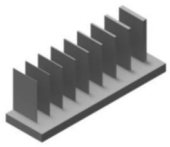	Wall thickness ≥0.3 mm	• 15 mm height with no deviation from the design if thickness ≥0.3 mm • Manufactured thickness max. 12% smaller for a thickness of 0.3 mm
Unsupported large walls	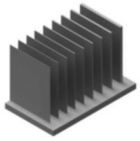	Wall thickness≥0.6 mm	• 30 mm height with no deviation from design
Supported walls	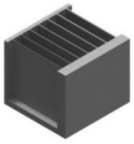	Wall thickness≥0.3 mm	• 30 mm height with no deviation from the design • 6% smaller target thickness
Inclined walls	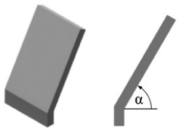	Overhang angle α 25°–80°	• Within this limit manufacturable • Upskin: mean roughness max. 90 μm for 25°and 73 μm for 80° • Downskin: mean roughness max. ~400 μm for 25° and ~60 μm for 80° angle
Horizontal overhang	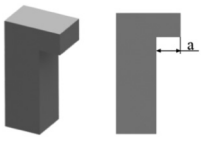	a ≤ 1.0 mm	• Overhang length greater than 1 mm should be supported because they tend to deform
Horizontal bridges	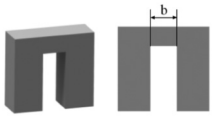	b < 3.0 mm	• All bridge spans buildable (1–5 mm) • Higher bridge span ≥3 mm should be supported to prevent a material fall-in
Unsupported bars	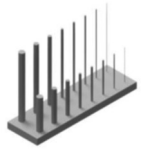	Diameter ≥0.8 mm	• Similar smaller bar diameter manufactured for 15 and 30 mm about 1%–2% • Bars tend to bend for d < 0.8 mm

TABLE IV. (*Continued.*)

Geometry feature		Recommendation	
Name	Illustration	Value	Comment
Horizontal bore holes	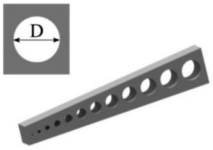	Diameter ≥4 mm, always support recommended	• Hole diameter of ≥4 mm preferred, less than 2% deviation in horizontal diameter • Material fall-in on the top; therefore, support structures should be used or tear drop shape
Horizontal tear drop features	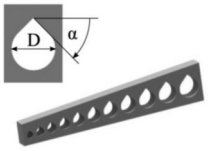	Diameter 5–15 mm	• for α = 30°, a material fall-in on the top of the tear drops ≥10 mm is observable; support structures should be used or increase α • for α = 45°, no support structure is necessary

IV. SUMMARY AND OUTLOOK

Selected design features have been built by L-PBF in IN718. Based on the results, general recommendations for the design of IN718 L-PBF parts can be derived that are mainly in line with similar investigations performed with different materials, such as Ti-6Al-4V. For example, free-standing walls should be oriented at an angle of at least 15° to the recoater direction, and tear drop shapes can effectively avoid the need for internal support structures. Besides, it was found that IN718 can be manufactured under rather steep inclination angles of up to 25°, although the roughness of the down-skin surfaces increases rapidly from 50° downward. Additionally, the design limits for the specific machine setup, process parameters, and powder were identified. The findings were applied to a large-scale engine frame that was optimized for weight and pressure loss. The concept was validated by successfully printing a segment of the part.

Several DfAM guidelines were used on the demonstrator:

- The minimum wall thickness was 1 mm (both for supported and unsupported walls).
- The minimum lattice wall thickness was 1 mm.
- Support structures were used if the boreholes were larger than 4 mm.
- Support structures were not used if the inclined wall overhang angles were within 50°.

It has to be noted that the transfer of the results to other machines and process parameters might produce slightly different design limits and, thus, should be experimentally confirmed case by case. Furthermore, upscaling to the 360° full-size component is foreseen to be investigated.

ACKNOWLEDGMENTS

Part of this work results from the project "MOnACO—Manufacturing of a large-scale AM component." This project has received funding from the Clean Sky 2 Joint Undertaking (JU) under Grant Agreement No. 831872. The JU receives support from the European Union's Horizon 2020 research and innovation program and the Clean Sky 2 JU members other than the Union. The results regarding combining laser powder bed fusion with hot isostatic pressing discussed in Sec. II originate from the project "Increasing the profitability of laser beam melting," C4T318, in the frame of the funding program "Calls for Transfer," financed by "Behörde für Wissenschaft, Forschung, Gleichstellung und Bezirke (BWFGB)" Hamburg and coordinated by Hamburg Innovation. The authors would like to express their gratitude for the funding. Also, the authors would like to thank Laurenz Plöchl, Johannes Gårdstam, and Jim Shipley of Quintus Technologies AB for conducting the Hot Isostatic Pressing (HIP).

APPENDIX: DESIGN GUIDELINE CATALOG

Design guidelines and recommendations for L-PBF of IN718 are shown in Table IV.

REFERENCES

[1]K. N. Amato, S. M. Gaytan, L. E. Murr, E. Martinez, P. W. Shindo, J. Hernandez, S. Collins, and F. Medina, "Microstructures and mechanical behavior of Inconel 718 fabricated by selective laser melting," Acta Mater. **60**, 2229–2239 (2012).

[2]F. Caiazzo, V. Alfieri, G. Corrado, and P. Argenio, "Laser powder-bed fusion of Inconel 718 to manufacture turbine blades," Int. J. Adv. Manuf. Technol. **93**, 4023–4031 (2017).

[3]M. Gralow, F. Weigand, D. Herzog, T. Wischeropp, and C. Emmelmann, "Biomimetic design and laser additive manufacturing—A perfect symbiosis?" J. Laser Appl. **32**, 21201 (2020).
[4]L. Nickels, "AM and aerospace: an ideal combination," Met. Powder Rep. **70**, 300–303 (2015).
[5]M. Kamal and G. Rizza, *Additive Manufacturing for the Aerospace Industry* (Elsevier, Amsterdam, 2019), p. 67.
[6]C. Emmelmann, D. Herzog, and J. Kranz, *Laser Additive Manufacturing* (Elsevier, Cambridge, 2017), p. 259.
[7]J. Kranz, D. Herzog, and C. Emmelmann, "Design guidelines for laser additive manufacturing of lightweight structures in TiAl6V4," J. Laser Appl. **27**, S14001 (2015).
[8]A. Ewald and J. Schlattmann, "Design guidelines for laser metal deposition of lightweight structures," J. Laser Appl. **30**, 032309 (2018).
[9]L. Rebaioli and I. Fassi, "A review on benchmark artifacts for evaluating the geometrical performance of additive manufacturing processes," Int. J. Adv. Manuf. Technol. **93**, 2571–2598 (2017).
[10]E. Hosseini and V. A. Popovich, "A review of mechanical properties of additively manufactured Inconel 718," Addit. Manuf. **30**, 100877 (2019).